T 形接头双光束激光焊变形计算方法

王学东，　何恩光，　钱红丽
（北京航空制造工程研究所 高能束流加工技术重点实验室，北京　100024）

王学东

摘　要： 以厚度为 2.5 mm 的铝锂合金 5A90 薄壁 T 形接头双光束激光焊变形为研究对象，针对焊缝金属熔化及凝固引起的材料力学行为变化，考虑筋板与底板之间连接的实现过程，开发了双光束激光焊单元生死温度判别法，焊接过程中以单元瞬态温度为判据，对单元动态杀死和激活；对比了采用与不采用单元生死温度判别法的焊接变形计算结果，该两种计算方法在材料参数、几何模型、边界条件及初始条件等方面都完全相同. 结果表明，是否采用单元生死温度判别法对 T 形接头双光束激光焊变形的计算结果有显著影响，并对这种影响进行了分析.

关键词： T 形接头；　双光束激光焊；　焊接变形
中图分类号： TG456.7　　**文献标识码：** A　　**文章编号：** 0253－360X(2013)11－0093－04

0　序　　言

近年来含 T 形接头的轻合金薄壁结构在航空领域[1]的应用不断增多，随之而来的是对其焊接变形的研究逐渐受到重视. 目前国内外对铝、钛合金薄壁 T 形接头双光束激光焊变形的研究还不多见[2,3]，多为其它焊接方法及钢铁材料[4,5]的 T 形接头焊接变形研究.

为准确计算铝合金薄壁 T 形接头的变形规律，考虑到焊接接头形成过程特点及单元生死技术在材料加工中的应用[1,6]，开发了单元生死温度判别方法，焊接过程中以单元瞬态温度为判据，对单元动态杀死和激活，对采用与不采用这种方法的 T 形接头焊接变形计算结果进行了对比和分析.

1　计算模型

双光束激光焊时，采用两束激光束在 T 形接头两侧对称施焊，激光束与板面呈一定角度，示意图如图 1 所示.

焊件材料为 5A90 铝合金，底板尺寸为 200 mm ×170 mm × 2.5 mm，筋板 200 mm × 37 mm × 2.5 mm，考虑到模型的对称性，建立一半模型如图 2 所示，材料参数设置为温度函数.

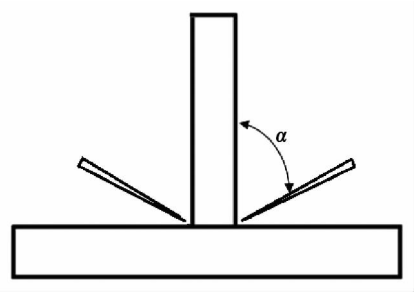

图 1　T 形接头双光束激光焊示意图
Fig. 1　Schematic of double beam laser welding of T joint

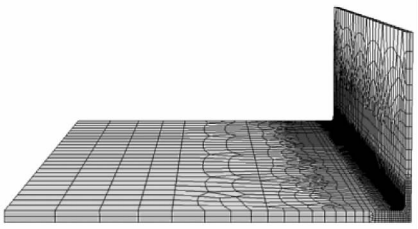

图 2　计算模型网格划分
Fig. 2　Finite element model and mesh

模型坐标系统如图 3 所示. x 为焊接方向，y 与焊接方向垂直，z 为竖直方向.

两种计算方法：(1) 采用单元生死温度判别法. (2) 不采用单元生死温度判别法. 方法 2 在焊接之前，筋板与底板实际为一整体，这种方法即常规的弹塑性有限元方法. 方法 1 由两个步骤组成. 焊接前杀死筋板与底板接缝处一薄层单元，但并未杀死全

收稿日期：2012－07－01
基金项目：高能束流加工技术重点实验室基金资助项目

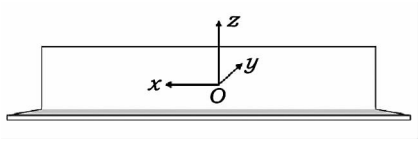

图 3 坐标系统

Fig. 3 Coordinate system

部焊缝单元，使得焊接之前筋板与底板并非一体，连接是随焊接过程逐步实现的，根据温度对焊缝单元进行杀死和激活，即温度高于材料液相线的单元被杀死，如图 4 所示，当被杀死的单元温度降至固相线以下时被激活. 两种方法，筋板与底板焊前都经过点固焊过程，采用两个点固焊点，每个焊点完成之后各有一段冷却时间. 除是否采用单元生死温度判别法外，两种方法在模型尺寸、网格划分、热源、边界条件等其它方面都完全相同.

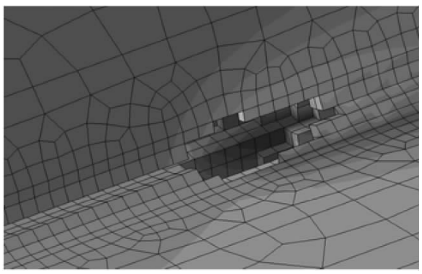

图 4 被识别出的熔池单元

Fig. 4 Molten elements identified

焊接过程中限制底板 z，x 向位移，坐标方向如图 3 所示，限制筋板顶部 z 向位移，以上拘束在焊接及冷却过程中保持，冷却至室温后去除.

2 计算结果

点固焊完成后的焊点状态如图 5 所示. 两种方法采用相同的焊接工艺参数，所获得的焊缝成形相同，如图 6 所示.

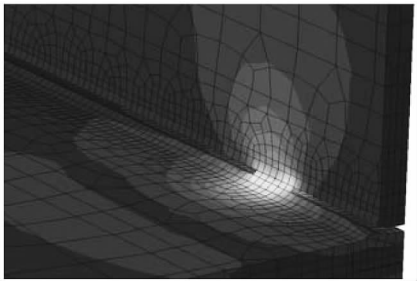

图 5 点固焊完成后的焊点

Fig. 5 Tack welding

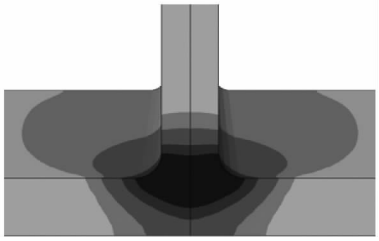

图 6 焊缝成形

Fig. 6 Schematic shape of weld

为比较焊接变形相对大小，在模型中取若干路径，如图 7 所示，O，O_1，O_2，O_3 等为各条路径的起点. 沿图 7a 所示直线取样，两种计算方法的 z 向位移如图 8a 所示. 沿图 7b 所示直线 1 筋板顶部位置取样，两种计算方法的 z 向位移如图 8b 所示. 沿图 7b 所示直线 2 的板侧边取样，两种计算方法的 z 向位移对比如图 8c 所示.

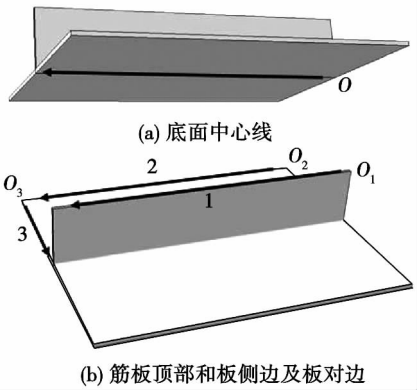

图 7 取样位置

Fig. 7 Sampling location

由图 8 的计算结果可以看出，对方法 1 和方法 2 各自而言，沿板底部中心线、筋顶部及板侧边等不同位置取样时，z 向位移方向都相同；但两种方法的 z 向位移方向相反. 方法 1 的 z 向变形都是向上凹，而方法 2 的计算结果都是向上凸.

沿图 7b 中直线 3 位置取样，两种方法角变形计算结果对比如图 9 所示. 由图 9 中可以看出，两种计算方法的角变形比较接近.

3 计算结果分析

前述两种计算方法的计算模型、焊缝成形及拘束条件等都相同，唯一的区别是方法 1 采用了单元

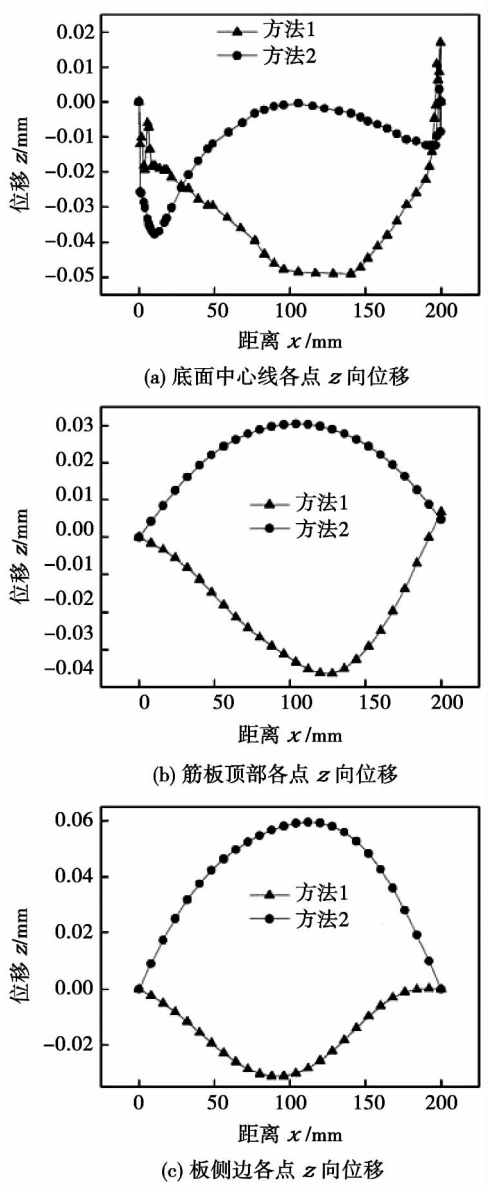

图 8　沿板底部中心线和筋板顶部及板侧边的 z 向位移对比

Fig. 8　z displacement along bottom center-line, top of stiffener and side edge

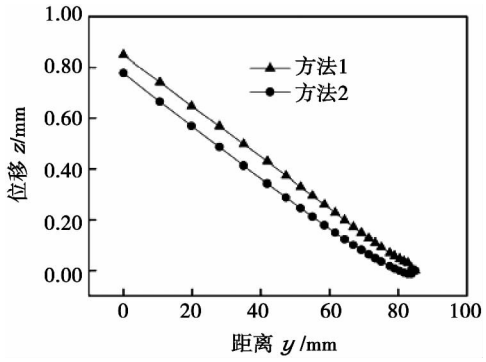

图 9　两种方法角变形对比

Fig. 9　Angular deformation of two computating methods

生死温度判别法，所得到的 z 向变形方向相反，原因分析如下.

T 形接头由筋板和底板组成，由于筋板与底板在尺寸、拘束、空间位置等方面存在不同，使得在焊接过程中二者的变形存在一定程度的不协调性. 采用方法 1 时，筋板与底板在焊接之前只通过两个焊点固定，而方法 2 的筋板与底板在焊接之前实际上是一体的.

对两种方法的收焊端进行观察可以发现，如图 10 所示，采用方法 1 时，收焊端筋板与底板之间并非平齐，筋板向外凸出，为便于观察，图 10 中将变形放大 10 倍显示. 方法 2 的收焊端筋板与底板之间是平齐的，未出现筋板凸出或凹入现象.

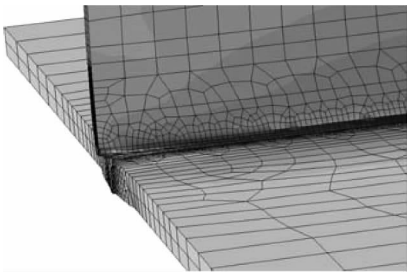

图 10　收焊端筋板凸出

Fig. 10　Protrusion of end of stiffener

通过对整个计算过程进行观察可以发现，采用方法 1 时，收焊端筋板端部所出现的凸出在点固焊之后不存在. 在连续焊接过程中，筋凸出点与板端点 x 向位移差与时间的关系如图 11 所示. 由图 11 中可以看出，位移差在焊接过程中动态波动，当焊接完成后，该位移差大于零，即形成筋的凸出，而方法 2 的位移差则始终为 0. 这种凸出只在收焊端出现，而在起焊端不出现，这是由于焊接过程中焊缝从起

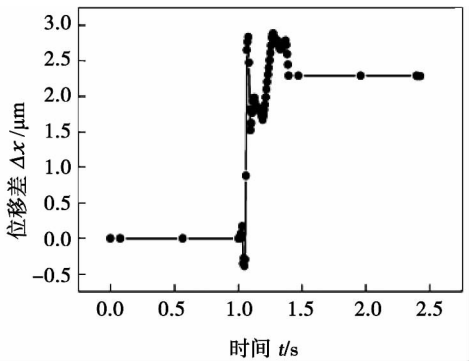

图 11　筋板和底板末端在焊接过程中纵向位移差

Fig. 11　Difference of longitudinal displacement between ends of stiffener and base plate versus time during welding

焊端向收焊端延伸，筋板与底板的连接亦从起焊端开始，向收焊端发展.

方法 2 筋板与底板在焊接之前为一体，而实际上只有当整条焊缝完成后约束才能达到这种状态，因此方法 2 对筋板和底板施加了附加约束.

为了证实以上分析，在采用方法 1 计算时，在原约束条件不变的基础上又对筋板侧面增加了 x 向位移约束(方法 3)，推测其变形方向应该与方法 2 相同，即 z 向变形向上凸. 计算结果如图 12 所示，变形方向与推测一致，但变形量比方法 2 更大. 对筋板所施加的 x 向位移约束是对筋板的整个板面施加的，这与方法 2 只是在接合面处存在约束不同，因此变形的大小也存在差异.

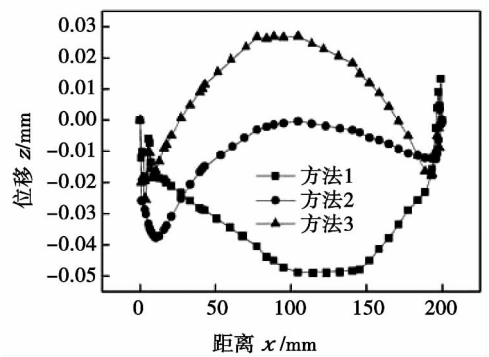

图 12 z 向变形对比

Fig. 12 z displacement of three computing methods

4 结 论

(1) 对于铝合金薄壁 T 形接头双光束激光焊，采用与不采用单元生死温度判别法，T 形接头挠曲变形的计算结果方向相反，分别为向上凹和向上凸，但角变形计算结果比较接近.

(2) 薄板 T 形接头由筋板和底板组成，焊接过程中筋板与底板变形的不协调性将影响接头最终的变形，采用方法 2 时会给 T 形接头带来附加约束，采用单元生死温度判别法可以避免这个问题.

参考文献:

[1] 李 昊，陈 洁，陈 磊，等. 双光束激光焊接技术在民用飞机上的应用现状及发展[J]. 航空制造技术，2012(21)：50－53.
Li Hao，Chen Jie，Chen Lei，*et al*. Application and development of double-beam laser welding technology in civil aircraft frabrication[J]. Aeronautical Manufacturing Technology，2012(21)：50－53.

[2] Muhammad Z，Daniel N，Jean-Francois J，*et al*. Experimental investigation and finite element simulation of laser beam welding induced residual stresses and distortions in thin sheets of AA 6056-T4[J]. Materials Science and Engineering A，2010，527：3025－3039.

[3] 刁旺战. 铝合金双光束激光填丝焊温度场与应力场数值模拟[D]. 哈尔滨：哈尔滨工业大学，2010.

[4] 黎超文，王 勇，韩 涛. 焊接顺序对 T 形接头残余应力和变形的影响[J]. 焊接学报，2011，32(10)：38－40.
Li Chaowen，Wang Yong，Han Tao. Influence of welding sequence on welding residual stress and deformation of T joint[J]. Transactions of the China Welding Institution，2011，32(10)：38－40.

[5] 闫得俊，刘雪松，周广涛，等. 大型底板结构焊接顺序控制变形数值分析[J]. 焊接学报，2009，30(6)：55－58.
Yan Dejun，Liu Xuesong，Zhou Guangtao，*et al*. Numerical analysis on optimizing welding sequence of large sized bottom structure for controlling welding distortion[J]. Transactions of the China Welding Institution，2009，30(6)：55－58.

[6] 胡军峰，杨建国，方洪渊，等. 电弧气刨温度场及其对微观组织的影响[J]. 焊接学报，2006，27(5)：93－96.
Hu Junfeng，Yang Jianguo，Fang Hongyuan，*et al*. Temperature field of arc gouging and its influence on microstructures[J]. Transactions of the China Welding Institution，2006，27(5)：93－96.

作者简介： 王学东，男，1969 年出生，博士，高级工程师. 主要从事激光加工方面的研究工作. 发表论文 20 余篇. Email：wxue2012@yeah.net

National Engineering Research Center for Commercial Aircraft Manufacturing, Shanghai 200436, China; 2. State Key Laboratory of Advanced Welding and Joining, Harbin Institute of Technology, Harbin 150001, China; 3. National Key Laboratory of Metal Precision Hot Processing, Harbin Institute of Technology, Harbin 150001, China). pp 73 – 77

Abstract: The behavior characteristics of wire melting and fiber laser beam welding process of aluminum alloys with filler wire were carried out by using high-speed camera and experimental tests. The filler wire melting behavior and its main influencing factors were analyzed. The effect of wire feeding mode and wire feeding angle on weld formation and welding process stability were also studied. The results show that the melting behavior, which mainly depends on the distance between laser incident position and filler wire, can be divided into three types: the spreading transfer, the liquid bridge transfer and the globular transfer, and the liquid bridge transfer is the ideal type. The mode of pre-wire has higher efficiency and wider process window. The level of laser energy absorption by wire and the impact force of liquid wires on the liquid weld pool are affected by the wire feeding angle. The back weld width increases obviously with increase of wire feeding angle, while the weld penetration keeps essentially invariable.

Key words: laser technique; melting dynamics; high-speed camera; aluminum alloys; wire parameters

Geometry quality prediction of Ni-based superalloy coating by laser cladding based on neural network and genetic algorithm YANG Youwen[1], TIAN Zongjun[1], PAN Hu[1], WANG Dongsheng[1,2], SHEN Lida[1] (1. College of Mechanical and Electrical Engineering, Nanjing University of Aeronautics and Astronautics, Nanjing 210016, China; 2. Department of Mechanical Engineering, Tongling College, Tongling 244000, China). pp 78 – 82

Abstract: Combination of back-propagation (BP) artificial neural network (ANN) and genetic algorithm was used to set up genetic neural network model to predict the quality of laser cladding layer according to the laser power, powder feed rate and scan rate. An orthogonal test was designed to obtain the training data of prediction model, and then the influence of different process parameters on the cladding layer geometry quality was analyzed by the method of range analysis. The validation results show that the relative error between predicted values and experimental data is less than 4.6%, which indicated that the use of the model can accurately select cladding parameters to improve the geometry quality of the laser cladding layer of nickel-based superalloy.

Key words: laser cladding; geometry quality; artificial neural networks; genetic algorithms; range analysis

Pulsed MIG welding of aluminum alloy sheet based on fuzzy self-tuning PID control ZHANG Xiaoli[1,2], LI Yuzhen[1], LONG Peng[1], XUE Jiaxiang[1] (1. School of Mechanical and Automotive Engineering, South China University of Technology, Guangzhou 510640, China; 2. School of Mechanical and Electrical Engineering, Jiangxi University of Science & Technology, Ganzhou 341000, China). pp 83 – 87

Abstract: A fuzzy self-tuning PID control method was proposed for pulsed MIG welding of aluminum alloy sheet. The principle and design ideas were introduced. Fuzzy self-tuning PID parameter was implemented by introducing the fuzzy logic controller into the established Simulink model of PID controller. Then input adaptability experiment contrast and anti-interference test were conducted and analyzed. It shows that fuzzy self-tuning controller in input adaptability and anti-interference is better and the arc welding power performance can be further improved. Finally the contrast of welding experiments on 1 mm thickness aluminum alloy between traditional PID control and fuzzy self-tuning parameter PID control were carried out. The experiments result shows that high welding quality and stable welding process with good weld seam, less welding spatter, relatively smooth welding process are achieved by the proposed method.

Key words: aluminum alloy sheet; PID control; fuzzy self-tuning; MIG welding

Microscopic feature of TC4 linear friction welded joints ZHU Jianqiao[1], ZHANG Yanhua[1], ZHANG Tiancang[2], SUN Chengbin[2] (1. Teaching and Research Section 702, Beihang University, Beijing 100191, China; 2. Research Section 102, Beijing Aeronautical Manufacturing Technology Research Institute, Beijing 100024, China). pp 88 – 92

Abstract: Microscopic features of TC4 linear friction welded joints were analyzed and the variation of the characteristic parameters with welding time was studied. The results indicated that the joint interface includes the welded zone, the transition zone and the incomplete bonding zone. Fine dynamic recrystallization grains appeared in the welded zone where the joint interface fused completely. Micro pores formed in the transition zone where the joint interface fused partly. In the incomplete bonding zone, metals on both sides of the joint interface were not contacted and grains were out of distortion. Moreover, metal fragments developed in the joint interface. Three-branch structure forms in the joint interface due to the separation of the vibration direction flash and the vertical vibration direction flash. Friction pressure and upsetting pressure are inclined to close the branches, while friction shear force attributes for expanding the branches.

Key words: linear friction welding; microscopic feature; micro pore; three-branch structure

Computational method for deformation of T joint welded by double beam laser WANG Xuedong, HE Enguang, QIAN Hongli (Key Laboratory of High Energy Density Beam Processing Technology, Beijing Aeronautical Manufacturing Technology Research Institute, Beijing 100024, China). pp 93 – 96

Abstract: The computational method of deformation of T joint of aluminum-Li alloy with thickness of 2.5 mm welded by double beam laser was studied. By taking account of the change of mechanical characteristics of the weld metal in heating, melting, cooling and solidifying process, and the forming process of the T joint, a method of calculating the deformation of T joint

welded by double beam laser welding was developed based on birth-death control by the temperature of each element. In the method, an element was killed or activated according to its temperature during welding. The welding deformation obtained by two different computational methods were compared, one using the birth-death control method, and the other not. Except the above difference, material, geometry, boundary and initial conditions were identical for the two computational methods. The results showed that, whether using the birth-death control or not, which had an important influence on the computational results of deformation of T joint welded by double beam laser welding, and the reason was analyzed.

Key words: T joint; double beam laser welding; welding deformation

Numerical simulation of temperature and flow field of CO_2 gas shielded arc XIA Shengquan, OU Zhiming, SUN Xiaoming (Key Laboratory for Advanced Materials Processing Technology, Tsinghua University, Beijing 100084, China). pp 97 – 100

Abstract: A transient three-dimensional model of welding arc in CO_2 gas shielded arc welding was founded. With the experimental data of transient welding current, the basic theory of magneto hydrodynamics (MHD) and the coupling of multi-physics function of ANSYS, the distribution of the current density in electric field, the electromagnetic force in magnetic field, the temperature and velocity in the flow field were simulated. The simulation result for arc temperature filed is basically identical with the experimental data in the reference. In addition, the laminar hypothesis and incompressible assumption in the model were verified by computing the Reynolds number and Mach number. The numerical model can provide theoretical guidance with the controlling of welding arc in the CO_2 gas shielded arc welding, and it also lays a foundation for the further study on the analysis of transient CO_2 arc.

Key words: welding arc; numerical modeling; multi-field coupling

Interfacial IMC evolution in micron Sn-Ag-Cu soldered joint during thermal aging TIAN Ye[1,2], WU Yiping[2], AN Bing[2], LONG Danfeng[3] (1. School of Mechanical and Electrical Engineering, Henan University of Technology, Zhengzhou 450001, China; 2. School of Materials Science and Engineering, Huazhong University of Science and Technology, Wuhan 430074, China; 3. Department of Precision Instruments and Mechanology, Tsinghua University, Beijing 100084, China). pp 101 – 104

Abstract: The interfacial intermetallic compound (IMC) evolution in micro-soldered joints in thermal aging process of flip-chip assemblies was investigated. The results show that all $(Ni,Cu)_3Sn_4$ on the Ni pad interface are transformed into $(Cu,Ni)_6Sn_5$ after 300 h for thermal aging due to the effect of Cu atoms diffused from the Cu pad interface on the $(Ni,Cu)_3Sn_4$. On the Cu pad interface, a thin layer of Cu_3Sn forms on the interface between the Cu pad and $(Cu,Ni)_6Sn_5$ after 100 h for aging, however in the subsequent thermal aging, Cu_3Sn experiences little growth because of the limitation effect of Ni on its growth. The growth rate of $(Cu,Ni)_6Sn_5$ on the both pad interfaces are fast before 100 h, and after 100 h, it become slower and slower. Furthermore, as the aging time increases, the interface of $(Cu,Ni)_6Sn_5$ grain inclines to be flat.

Key words: lead-free solder; intermetallic compound; flip chip assembly; interfacial reaction; thermal aging

Research on A-MAG welding of weathering resistant steel LU Hao[1], XING Liwei[2], CHEN Dajun[3] (1. Technical Engineering Department, CSR Qingdao Sifang Co., Ltd., Qingdao 266111, China; 2. Technology Center, CSR Qingdao Sifang Co., Ltd., Qingdao 266111, China; 3. Harbin Welding Training Institute, Harbin 150046, China). pp 105 – 108

Abstract: A-MAG welding was proposed to obtain the welded joints with high quality. The experiment results show that A-MAG weld appearance, internal quality of welded joint and the welding operation performance are very well. Experiments also show that the A-MAG welding can improve weld penetration, which is compared with MAG welding under the same heat input. The tensile strength and bending strength of A-MAG welded joint are not reduced, while impact strength is improved, especially in the HAZ. Dimples size in fracture appearance of A-MAG welded joint is finer. It is showed that the active MAG welding can improve the welding quality and weld penetration of weathering resistant steel, which is applicable in engineering application.

Key words: A-MAG welding; weathering resistant steel; high speed train

Grain types and composition distribution of agglomerated flux with high slag detachability XU Guoliang[1], ZHENG Zhentai[1], LIU Pengfei[2], ZHANG Lisheng[1], WANG Tao[1] (1. School of Materials Science and Engineering, Hebei University of Technology, Tianjin 300132, China; 2. Luo Yang Institute of Ship Materials, Luoyang 471023, China). pp 109 – 112

Abstract: In order to enhance slag detachability of agglomerated flux for low-alloy steel in root bead, uniform design method was used to optimize slag systems for MgO-Al_2O_3-CaO with high basicity and slag detachability test. Then scanning electron microscopy (SEM), energy dispersive x-ray analysis (EDAX) and X-ray diffraction (XRD) were used to analyze the microstructure, compositions and phase of slag. The results show that the No. 10 slag with higher detachability is mainly made of compound rock phases, whose main elements are Zr, Mg, Ca, Al and Si. Since the element content is different in slag microzone, it can form snowflake grain with Zr, cross grain with Mg, and dentrite with Ca. Dentrite with Ca and snowflake grain with Zr can hinder the growth of cross grain with Mg. In addition, Zr has a role in refining cross grain with Mg. So the increase of the contents of marble and zircon sand in flux can change the continuity and direction of cross grain with Mg in slag. It will be a valid way to improve slag detachability.

Key words: agglomerated flux; microstructure; composition distribution; slag detachability